This is the accepted manuscript made available via CHORUS. The article has been published as:

Understanding the role of grafted polystyrene chain conformation in assembly of magnetic nanoparticles

Yang Jiao and Pinar Akcora

Phys. Rev. E **90**, 042601 — Published 17 October 2014

DOI: 10.1103/PhysRevE.90.042601

Understanding the Role of Grafted Polystyrene Chain Conformation on Assembly of Magnetic Nanoparticles

Yang Jiao and Pinar Akcora*

Department of Chemical Engineering & Materials Science
Stevens Institute of Technology, Hoboken, NJ 07030 USA

* Corresponding author. pakcora@stevens.edu

Polystyrene-grafted iron oxide nanoparticles have been shown to phase separate into ordered morphologies of strings, well-dispersed particles and spherical aggregates at low graft densities in polymer matrices. In this work, small-angle neutron scattering experiments are performed to reveal the role of grafted chain conformation on nanoparticle assemblies. We demonstrate that chains grafted at low densities follow Gaussian statistics at any dispersion states. These results suggest that grafted chains are not distorted but remain Gaussian when particles are aggregated into strings. Small-angle X-ray and neutron scattering results show that matrix chains do not influence the formation of strings, but have a significant impact on the size and internal structure of aggregated particles. We conclude that spherical aggregates of nanoparticles with low polymer graft densities are akin to interpenetrating networks in which free matrix chains bridge the fractals of particles and control the cluster density.

I. INTRODUCTION

The collective properties of polymer nanocomposites depend strongly on the organization of nanoparticles. While uniform dispersion can be ensured with physical adsorption of polymer chains on particles [1-3], anisotropic structures can only be obtained when nanoparticles are chemically modified at low densities with polymers [4-6]. In the case of particles that are physically adsorbed with chains, strong attractive interactions between a polymer matrix and bare particles lead to uniform and individual particle dispersions at loadings as high as 30 wt% [3,7]. It is also shown that polymer size (R_g) is not affected with the existence of particles in such mixtures [7]. In grafted systems, on the other hand, it has been recently proposed that Gaussian conformation of grafted chains can be distorted when particle cores approach due to particle-particle attractions [5]. Previous simulations indicate that steric crowding of grafted chains is the primary reason of chain-like aggregation [8], but there is no theoretical work or experimental evidence reporting any change in the size of grafted chains (*i.e.* expansion or stretching) when particles aggregate into strings. At low graft densities, enthalpic and entropic interactions compete within strongly attracting particles and lead to anisotropic aggregation of fillers where long-range repulsion competes with short-range attraction between nanoparticles [5,9,10]. Thus, the role of polymer conformation on equilibrium nanostructures is critical to corroborate the assembly mechanism of polymer-grafted nanoparticles which, in turn, governs structural stability and mechanical performance of polymer nanocomposites.

In this work, we investigate how grafted chains are conformed within different aggregation states of nanoparticles. Using small-angle neutron scattering (SANS) technique, we directly measure the conformation of grafted chains on iron oxide (magnetite, Fe_3O_4) nanoparticles since neutron

scattering length density (SLD) of magnetite cores can be nicely contrast matched with that of matrix polymer of deuterated polystyrene (d-PS). By combining information on particle structures in bulk composites obtained in transmission electron microscopy (TEM), small-angle X-ray scattering (SAXS) and SANS, we will examine whether chain conformations, hence entropic elasticity of chains, control the formation of strings and influence the packing of nanoparticles in spherical aggregates. Measuring the size of grafted chains within these different grafted-particle structures is the main focus of this study.

Previous works on SANS of grafted nanoparticles in composites reported that grafted chain conformations at high graft densities followed Gaussian statistics [11] and grafted chains were collapsed as particles formed aggregates [12]. In another work by Chevigny [13], SANS experiments have confirmed the wet-to-dry conformational transition of brush when particles were mixed with matrix molar masses that are lower and greater than the mass of grafted chains. Theodorou has simulated single chain and corona scattering for different surface densities and graft lengths [14]. Their simulation results, however, did not validate the collapse of corona observed in high molar mass matrices as reported in the experimental findings of Chevigny [13]. In another study, grafted particles at high graft densities in solution gave rise to extended chain conformations in the concentrated particle brush regime; and chains show Gaussian in semi-dilute particle brush regime [15]. Hore et al.'s recent work has shown that the concentrated polymer brush and semi-dilute polymer regions existed on PMMA-grafted Fe_3O_4 nanoparticles dispersed in deuterated PMMA matrix [16]. A quantitative agreement on brush conformation in composites and structure of polymer chains in solution has been shown for the highly grafted nanoparticles.

Herein, we report the variations in R_g of grafted chains in a PS-grafted Fe_3O_4 system (Fig. 1) with low graft densities. The hydrophobic nature of both core and grafts makes our system interesting since string formation in PS-grafted Fe_3O_4 nanoparticles [6] has different origins than the anisotropic assembly observed in the amphiphilic PS-grafted silica nanoparticles [5]. We analyzed our SANS data by the Pederson model [17] with an excluded volume term by using an appropriate particle form factor for different structures. SANS results reveal that grafted chains are unperturbed Gaussian chains within strings of magnetic particles at low (0.016 chains/nm^2) and intermediate (0.071 chains/nm^2) graft densities. Contrary to what is reported for the aggregates [12], here we demonstrate that chains on aggregated particles have Gaussian behavior at low graft density (0.057 chains/nm^2). More importantly, free chains are found to play a prominent role in the aggregated structures. These findings unite the structural information from polymer and particle parts and will help us to better understand the dynamics of grafted nanoparticles under shear flows where strings were aligned and clusters were mixed with free chains under shear [18]. It has been shown with Rheo-SANS experiments that polystyrene melts remain undeformed under steady shear [19], however it can be possible that grafted chains may be distorted and interpenetration of matrix chains into particle clusters can be facilitated with application of shear. SANS measurements on grafted chain conformations after applying shear will be the focus of a future work.

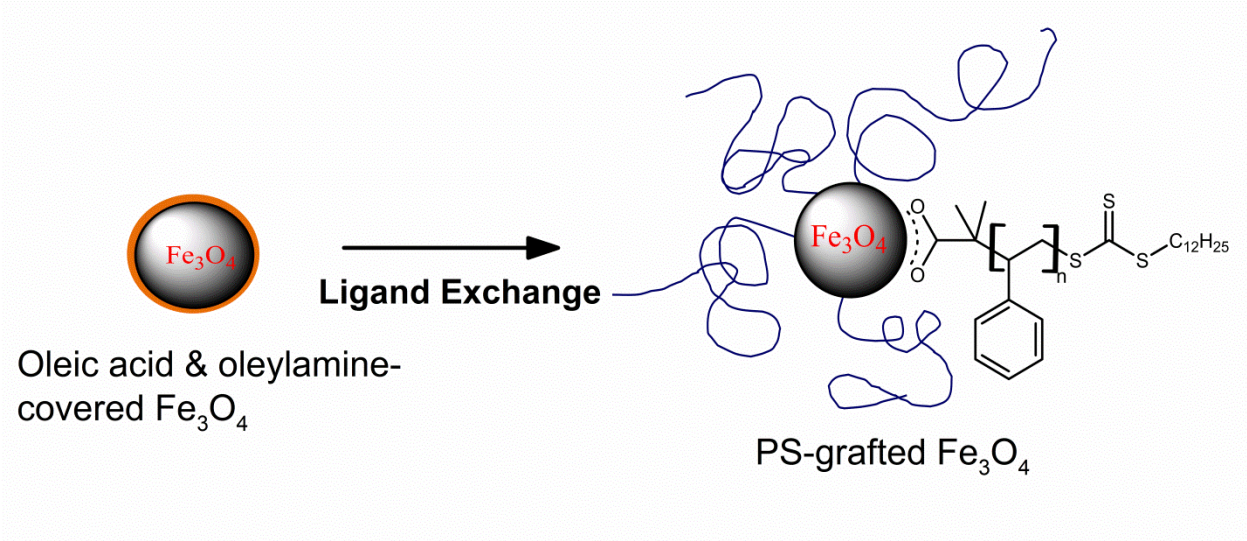

FIG. 1. (Color online) Schematic illustration of oleic acid and oleylamine covered Fe_3O_4 nanoparticles and their PS-grafted forms after ligand exchange reaction.

II. EXPERIMENTAL

A. Preparation of polystyrene-grafted nanoparticles and their bulk films

Oleic acid and oleylamine-stabilized Fe_3O_4 nanoparticles (NPs) were synthesized by a high-temperature thermal decomposition method [20]. Both protonated (h-PS) and deuterated polystyrene (d-PS) were prepared by reversible addition-fragmentation chain transfer (RAFT) polymerization [6,21] using 2-[(dodecylsulfanyl)-carbonothioyl]sulfanyl propanoic acid (DCSPA) as a chain transfer agent [22]. h-PS chains were grafted to surfaces of Fe_3O_4 NPs with different graft densities and molecular weights [6]. Table 1 lists molecular weight, dispersity, calculated ideal radius of gyration ($R_{g,theo}$), particle radius ($R_{particle}$), graft density obtained from thermal gravimetric analysis and volume ratio of grafted chains to particles for the synthesized h-PS-grafted NPs. Matrix polymer characteristics and structures formed by different aggregation states of particles, verified in TEM, are presented in Table 2.

Composite samples were prepared by mixing grafted NPs with d-PS homopolymer in toluene. Samples in solution were cast into Teflon dishes, dried in air and then annealed for 48 h in a vacuum oven at 150 ^{o}C to prepare ~1 mm thick films. Particle concentration in all composites was 5 wt%.

TABLE 1. Characteristics of synthesized h-PS grafted Fe_3O_4 NPs.

	Grafted Polymer			Particle Core	Graft density		Volume ratio of chains to core
Sample name	$\overline{M}_w$ **(kg/mol)**	**Dispersity,** $Đ$	$R_{g,theo}$ **(nm)**	$R_{particle}$ **(nm)**	**(chains/nm^2)**	**(chains/ particle)**	
100-0.016	119	1.07	9.5	5.2 ± 0.57	0.016	5	3.1
100-0.071	95	1.07	8.5	3.65 ± 0.34	0.063	10	7.3
43-0.057	43	1.11	5.7	3.65 ± 0.34	0.057	9	2.6
43-0.096				3.68 ± 0.06	0.072	14	4.4

TABLE 2. Molecular weights and dispersities of d-PS matrix polymers used in nanocomposites. Representative TEM micrographs of composite structures are displayed in Figure 1.

Sample name	**d-PS Matrix**		**Structure**
	$\overline{M}_w$ **(kg/mol)**	$Đ$	
100-0.016	51.6	1.09	strings
100-0.071	84.2	1.08	
43-0.096	32.2	1.09	well-dispersed
43-0.057	32.2	1.09	aggregates
	84.2	1.08	aggregates

B. Characterization

Molecular weights were determined by gel permeation chromatography-light scattering (GPC/LS) using a system equipped with a VARIAN PLgel 5.0 μm Mixed–C gel column (7.5 mm ID), a light detector (miniDawn, Wyatt Technology) and a refractive index detector (Optilab rEX, Wyatt). Nanocomposite films were microtomed into ~ 80 nm slices with a diamond knife at room temperature and examined in transmission electron microscopy (FEI CM20 FE S/TEM) operated at 200 keV. Many cross-sectional TEM images were captured over different areas for representative nanostructures.

Thermal Gravimetric analysis (TGA) was performed on a Q50 TGA (TA Instruments). Measurements were performed under a constant flow of nitrogen of 20 mL/min at a heating rate of 20 °C/min, starting from room temperature up to 580 °C, and then held constant at maximum temperature for 30 min. Graft density (σ) is calculated by: $\sigma = (\frac{\omega_{PS}}{100-\omega_{PS}} - \frac{\omega_0}{100-\omega_0}) R_{particle} N_A \rho_{Fe_3O_4} / (3\bar{M}_n)$, where ω_{PS} and ω_0 are the weight losses of PS-attached and bare particles, respectively; N_A is Avogadro constant, and $\rho_{Fe_3O_4}$ is density of Fe_3O_4.

1. Small-Angle X-ray Scattering (SAXS) measurements on composite films

SAXS measurements were performed at Beamline X27C at the National Synchrotron Light Source (NSLS), Brookhaven National Laboratory. The incident beam wavelength (λ) was 1.371Å and monochromatized using a double-multilayer (silicon/tungsten) monochromator. The sample to detector distance was 1.8 m. A Mar-CCD X-ray detector was used for data collection. The angular position of SAXS patterns was calibrated using a silver behenate standard. Data sets

were reduced from 2D to 1D format by integrating over 2θ using the Polar software (Stonybrook Technology and Applied Research (STAR) Inc., Stony Brook, NY). Air background pattern was collected for each sample environment, for a collection time equal to that of the sample. Each sample pattern was divided by their transmission, and then corrected by subtracting the air background pattern.

2. Small-Angle Neutron Scattering (SANS) measurements on nanocomposite films

SANS was performed on the NG3 30 m SANS instrument at the National Institute of Standards and Technology, Center for Neutron Research (NCNR, Gaithersburg, MD). SANS measurements were taken for three sample-to-detector distances of 1, 4 and 13 m. The neutrons had wavelength of λ = 6 Å at 1 and 4 m detector distances, and λ = 8.4 Å at 13 m detector distance. Standard data acquisition and data reduction techniques were performed to obtain radially averaged SANS data. The scattering pattern was reduced and analyzed using the Igor Macros package developed by the NIST Center for Neutron Research [21,23]. The correction for void scattering is applied by using the data of d-PS film containing ungrafted particles (see Appendix A on void scattering analysis). A low-q upturn in the scattering intensity with a slope of -4 is shown in Fig. S1, which is commonly attributed to scattering from voids in nanocomposites. Fig. S1 also shows the data profiles of composites before and after subtracting void scattering.

3. SANS data analysis of hPS-grafted particles in d-PS matrices

SLD of Fe_3O_4 particles (6.94 x10^{-6} Å^{-2}) matches to the SLD of deuterated PS matrices (6.52 x10^{-6} Å^{-2}), thus scattering arises purely from h-PS grafted chains (SLD: 1.41 x10^{-6} Å^{-2}). For dispersed system and strings, a polymer excluded volume model [24] (see Appendix B for equations) is used to describe the form factor of a single grafted chain, $P_{chain}(q)$, with two fitting

parameters: R_g and m ($1< m <3$). m is the inverse of excluded volume parameter (ν), and it depends on the dimensionality of a self-correlated system. For chains of finite length, scattering scales with q as $I(q) \sim q^{-1/\nu}$, where ν = 0.5 is for an ideal chain, ν = 0.588 is for a swollen chain in good solvent and ν = 1/3 is for collapsed globular conformation in bad solvent. The Pederson model [17,25] describes a spherical particle core attached with N_g number of chains. Thus, it includes correlation terms between a grafted chain and core ($S_{core\text{-}chain}$), and correlations between chains on the same particle ($S_{chain\text{-}chain}$). The Pederson form factor $P_{Pederson}(q)$ is given as[23]:

$$P_{Pederson}(q) = V_{core}{}^2 \Delta\rho_{core}{}^2 P_{core}(q) + N_g V_{chain}{}^2 \Delta\rho_{chain}{}^2 P_{chain}(q) + N_g(N_g-1) V_{chain}{}^2 \Delta\rho_{chain}{}^2 S_{chain-chain}(q) + 2N_g V_{core} V_{chain} \Delta\rho_{chain} \Delta\rho_{core} S_{core-chain}(q)$$

The scattering intensity $I(q)$ is expressed by: $I(q) = P_{Pederson}(q) + A_{mic}{}^{av}(q)^2[S(q)-1]$, where $A_{mic}{}^{av}$ is the scattering amplitude and $S(q)$ is the inter-structure factor of hybrid particles [25]. In dispersed systems with noninteracting units of individual particles and strings, $S(q) \approx 1$; thus the scattering equation simplifies to $I(q) = P_{Pederson}(q)$. Sphere and cylinder form factors, $P_{core}(q)$, were used for well-dispersed particles and strings, respectively. Structure and form factors of a sphere and a cylinder (P_{core}, P_{chain}, $S_{core\text{-}chain}$ and $S_{chain\text{-}chain}$) in the Pedersen model [26] are defined in the Appendix B. For aggregating systems, the Beaucage unified equation [27,28] is used to analyze SANS data.

III. RESULTS

By dispersing h-PS-grafted particles in d-PS matrices, we study brush chain conformations in SANS and examine the effect of matrix molecular weight on structures. Fig. 2 shows the

dispersion states of Fe_3O_4 nanoparticles grafted with 43 and 100 kg/mol PS at different graft densities. Short strings are seen in the 100k samples, and clusters and single particle dispersion are obtained in the 43k samples by varying the graft density from 0.057 to 0.096 chains/nm^2. We have reported similar anisotropic structures of PS-grafted iron oxide particles in our previous work [6]. String formation in our hydrophobic particles grafted with hydrophobic chains was attributed to entanglements between long grafts and the effective core-core interactions arising from dipolar and van der Waals forces. The shorter graft chains with the short-range repulsion, on the other hand, formed strings that were aggregated into branched chains [6]. In this work, by measuring the sizes of long (100 kg/mol) and short (43 kg/mol) PS grafted chains at low graft density in nanocomposites of different morphologies, we reconcile the role of grafted chain repulsion as they interact through penetration of free chains into grafts. We focus first on SAXS results for data presented in Fig. 2.

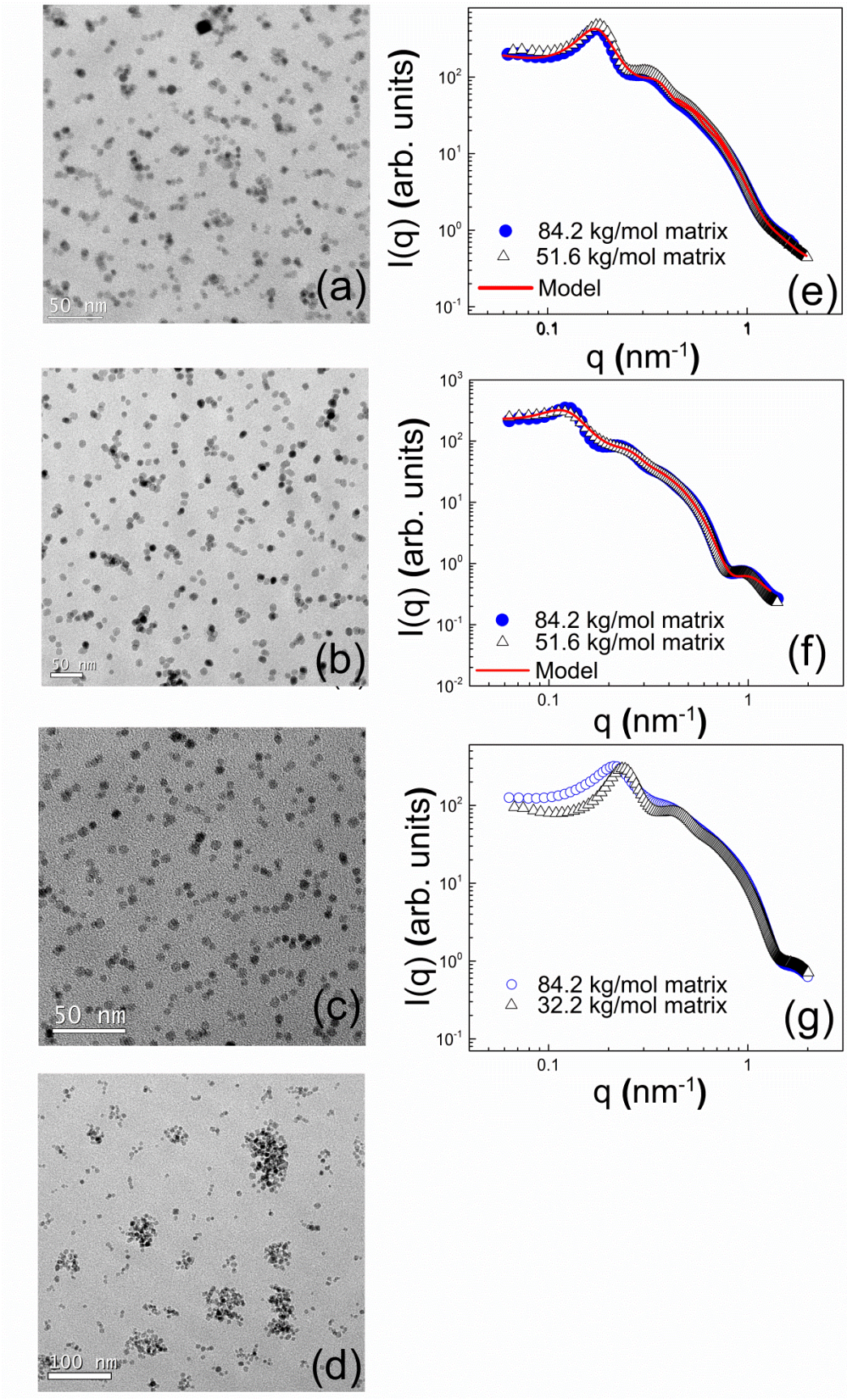
(a)
50 nm
(b)
50 nm
(c)
50 nm
(d)
100 nm
I(q) (arb. units)
q (nm^{-1})
84.2 kg/mol matrix
51.6 kg/mol matrix
Model
(e)
84.2 kg/mol matrix
51.6 kg/mol matrix
Model
(f)
84.2 kg/mol matrix
32.2 kg/mol matrix
(g)

FIG. 2. (Color online) TEM images of hPS-grafted Fe_3O_4 NPs in 84 kg/mol d-PS matrices at low and intermediate graft densities (a) 100-0.071, (b) 100-0.016, (c) 43-0.096, (d) 43-0.057; and SAXS profiles (e-g) of the corresponding composites in two different matrices. Red solid lines are the simulated model. Dispersion of the same particles in lower d-PS matrices can be found in Fig. 7. SAXS curves of the sample 43-0.057 are displayed in Fig. 5 for further discussion.

All composites excluding the 43-0.057 sample exhibit SAXS patterns with correlation peaks at small angles (Fig. 2), which correspond to ~25 and 30 nm average spacing between strings and individually dispersed particles, respectively. We explain the low-q peak in the dispersed system (of 43-0.096 sample in Figure 2g) with the steric repulsion of grafted chains, as this distance is equivalent to the calculated length of two grafted chains of 43 kg/mol. Such disordered but isolated particles are considered to be fractal-like structures since the grafted layers are percolated in this postulated morphology. Similarly, strings are analogous to fractal-like objects consisting of spherical building units with highly correlated intra-particle distances. We simulated scattering data by applying Percus-Yevick potentials to fractal structures of particles in strings and dispersed systems. It is known that disordered arrangements of spherical domains can be modelled with a Percus-Yevick hard sphere model [29,30] from which the hard sphere interaction distances, R_{HS}, and the effective volume fraction of the objects can be obtained. Total intensity is then expressed by $I(q) = P_{polysphere}(q)S_{fractal}(q)S_{P-Y}(q)$, where fractal structure factor, $S_{fractal}$, is for intra-structure and $S_{P\text{-}Y}$ is for inter-cluster structure correlations, and $P_{polysphere}$ is the sphere form factor with Gaussian size distribution. Scattering features at high-q regions arise from the primary particle structure and fit to a polydisperse sphere form factor [27], which is calculated as: $P_{polysphere}(q) = \int f(R, R_{avg}, \sigma)P_{sphere}(q, R)dR$, where

$P_{sphere}(q,R)=[\frac{3\sin(qR)-qRcos(qR)}{(qR)^3}]^2$ is the sphere form factor and $f(R,R_{avg},\sigma)=\frac{1}{\sigma\sqrt{2\pi}}\exp\left[-\frac{1}{2\sigma^2}(R-R_{avg})^2\right]$ is the Gaussian distribution, where R is the radius of the sphere, R_{avg} is the mean radius and σ is the polydispersity. R_{avg} and dispersity values obtained from the form factor analysis are shown in Table 3. $S_{fractal}$ is defined as [31]: $S_{fractal}(q)=1+\frac{\sin[(D_f-1)\tan^{-1}(q\xi)]}{(qR_{avg})^{D_f}}\frac{D_f\Gamma(D_f-1)}{[1+1/(q^2\xi^2)]^{(D_f-1)/2}}$, where D_f is the fractal dimension, ξ is the correlation length and Γ is the gamma function. $S_{P\text{-}Y}$ interference structure expression is described in Appendix B. The model of fractals interacting with hard sphere potentials fits nicely to the scattering data of strings as illustrated by red lines on SAXS curves. Table 3 summarizes the SAXS model fitting parameters. In 100k samples, the fractal dimension (D_f) increases from 2 to 2.3 as graft density decreases from 0.071 to 0.016 chains/nm^2, implying that particles form more compact structures at 0.016 chains/nm^2. The correlation length (ξ) is ~ 18 nm, which suggests that the basic unit of assembly is a trimer or tetramer. Particles tethered with short chains, 43k samples, exhibit similar structures in different matrix molecular weights, but with smaller correlation lengths (ξ = 7 nm in 32 kg/mol matrix and ξ = 9 nm in 84 kg/mol matrix) than that of 100k samples. The thickness of the corona, calculated by subtracting particle radius (R_{avg}) from hard sphere interaction distance (R_{HS}), is found to be 14.6 nm for 100-0.071, 18.8 nm for 100-0.016, and 11 nm for 43-0.096, which is close to $2R_{g,theo}$ of their corresponding grafted chains. The volume fraction of hard spheres is predicted as ~ 26-30% from the model that is larger than the volume of grafted particles (as listed on Table 1). Thus, from R_{HS} values, we conclude that the corona layer should contain free polymer at 18 and 20 vol% for 100-0.016 and for 43-0.096, respectively, which indicates good miscibility of grafts with the matrix.

TABLE 3. SAXS model parameters for composites with strings and well-dispersed NPs.

Sample	Matrix molecular weight (kg/mol)	$P_{particle}(q)$	$S_{fractal}(q)$		$S_{P\text{-}Y}(q)$	
		R_{avg} (nm)	D_f	ξ (nm)	R_{HS} (nm)	volume fraction
100-0.071	84.4	2.87 ± 0.27	2	18	17.5	0.30
	51.6					
100-0.016	84.4	5.2 ± 0.57	2.3	18	24	0.22
	32.2					
43-0.096	84.4	2.9 ± 0.05	1.9	9	13.9	0.26
	32.2		2.1	7	13.8	0.26

For finite-size objects, the number of aggregates (N_{agg}) could be approximately calculated from the shift of the intensity at low q plateau using $N_{agg} = I_{q\to 0}(q) / P_{sphere}(q)$. P_{sphere} is the monodispersed sphere form factor as defined in the previous section. Dimers (N_{agg} = 2) and trimers (N_{agg} = 3) are found in 100k samples, which seem to be slightly smaller than the string lengths seen in our TEMs (Fig. 1, top images). Single particle dispersion (N_{agg} = 1) is confirmed in 43-0.096 sample. Our SAXS analysis, thus, provides more reliable information on particle distribution than TEM based dispersion analysis.

Next, we analyzed SANS data of the composites by the Pederson model [17,25] which describes a sphere particle core grafted with N_g number of Gaussian chains. We replaced the Gaussian chain model by an excluded volume model (see Experimental). Particle sizes (R_{avg}) obtained from SAXS are used in the Pederson fits. Knowing the graft density and volume ratio of grafted PS to particle core obtained from TGA (values shown in Table 1), V_{chain} is calculated and kept constant. The fitting parameters in the modified Pederson model are: R_g, N_g and excluded volume parameter ($\nu = 1/m$) are given in Table 3. Note that scattering mismatch between particle core and d-PS should have minimal contribution to scattering data as the ratio of scattering density

differences between core-matrix and chain-matrix, $\Delta\rho_{core}{}^2 / \Delta\rho_{chain}{}^2 \approx 0.006$, is significantly small.

SANS profiles of 100 kg/mol PS-grafted particles (0.016 and 0.071 chains/nm^2) are nearly identical as shown in Fig. 3. The best fits in all four samples are obtained when $N_g = 1$ ($S_{chain\text{-}chain} = 0$) and the correlation term of a grafted chain with particle core ($S_{core\text{-}chain}$) is negligible. It is found that grafted chains on string structures behave as an ideal Gaussian chain with $\nu \sim 0.5$. We also note that R_g's determined from Pedersen fits with excluded volume chain form factor are close to the theoretical Gaussian size of 119 and 95 kg/mol PS chains (note the molecular weight differences for the 100k-labeled samples in Table 1). In our past work, we showed that varying matrix molecular weight did not influence the primary string structures [6]. Here, we reconcile this result with the unchanged R_g values of grafted chains in 51 and 84 kg/mol matrices (Table 4).

TABLE 4. Pederson fitting parameters for 100 kg/mol PS-grafted chains in d-PS matrices at low and intermediate graft densities.

Sample Name	$\overline{M}_w$ **(kg/mol) d-PS matrix**	R_g **(nm)**	N_g	***m***
100-0.016	51	12.5	1	1.90
	84	11.0	1	2.00
100-0.071	51	9.0	1	1.90
	84	8.7	1	1.95

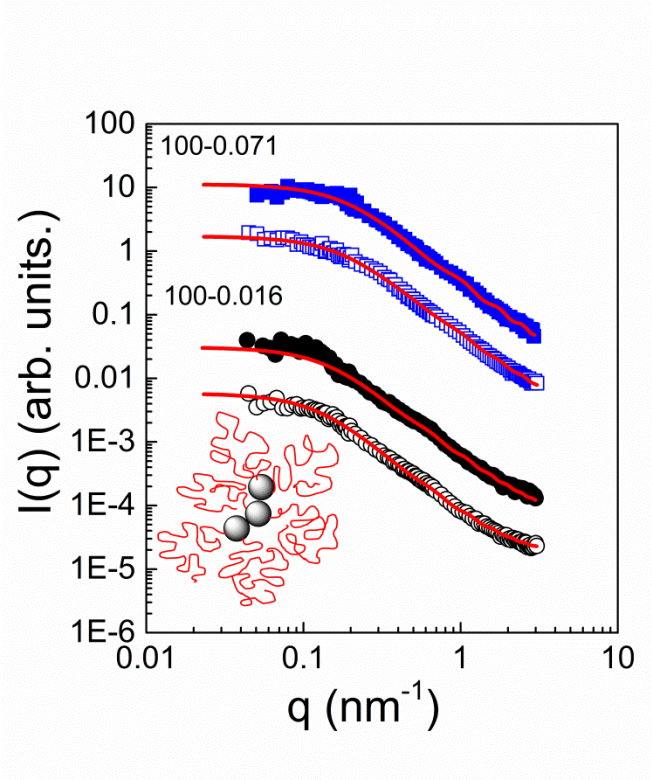

FIG. 3. (Color online) Measured SANS profiles of 100 kg/mol PS-grafted Fe_3O_4 NPs forming strings at 0.016 (black symbols) and 0.071 (blue symbols) chains/nm^2. Two sets of data are presented for particles dispersed in 51 kg/mol (open symbols) and 84 kg/mol (filled symbols) d-PS matrices. Red solid lines are the Pederson fits. Curves are shifted vertically for clarity.

TEM results indicate that grafting density plays a critical role in controlling morphology of nanoparticles with short graft chains (43 kg/mol). We showed that particles are well-dispersed at 0.096 chains/nm^2 and aggregate into spherical clusters at 0.057 chains/nm^2. Fig. 4 shows SANS profiles of the dispersed system (43-0.096) with their Pedersen fits. The fitting parameters in Table 5 suggest that the chains are all Gaussian. N_g, which is the number of chains on a particle, could be utilized as an index to describe not only the degree of chain-chain correlation, but also the interaction between grafted and free chains. The higher value of N_g may be due to the dewetting of chains in 84 kg/mol matrix. Additionally, we note that the interference peaks

around 0.15 nm^{-1} in SANS profile arise from uniform shielding of chains around particles in the well-dispersed system. The small feature at 1 nm^{-1} may come from the scattering of thin surfactant layers, which is more apparent for ungrafted particles as discussed in Fig. S1. Thickness of surfactant layer is only a few angstroms, and could be evaluated by adding a shell layer around particles in fitting, however this would not affect the fitting results of our work.

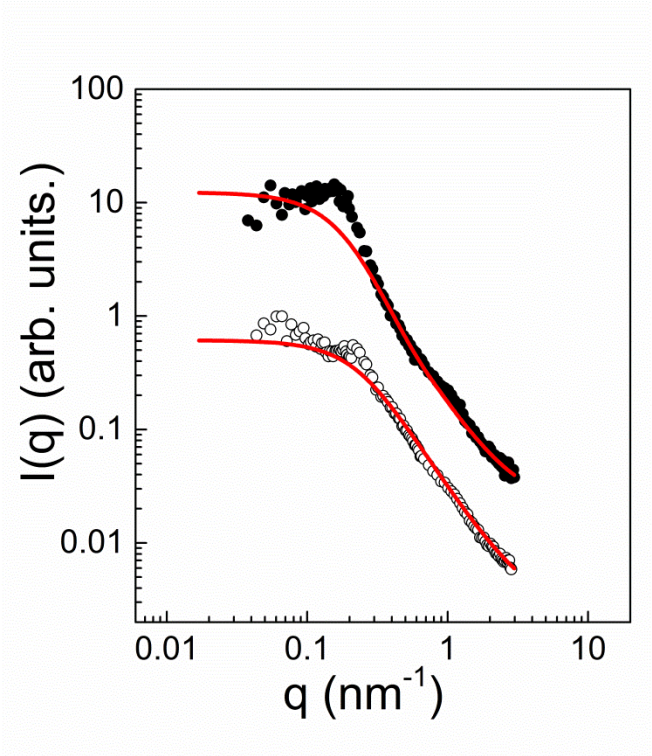

FIG. 4. (Color online) SANS profiles of 43 kg/mol PS-grafted nanoparticles with 0.096 chains/nm^2 in 84 (closed symbols) and 32 kg/mol (open symbols) d-PS matrix. Red solid lines are the Pederson fits. Curves are shifted vertically for clarity.

TABLE 5. Fitting parameters for 43 kg/mol PS-grafted chains in d-PS matrices at low and intermediate graft densities.

Sample Name	$\overline{M}_w$ (kg/mol) of d-PS matrix	R_g (nm)	N_g	m
43-0.057	32 84	5.6 (Beaucage) 5.6	-	2 1.97
43-0.096	32 84	6.8 (Pedersen) 6.4	1 4	1.94 1.94

Sample 43-0.057 is the only sample exhibiting spherical aggregates. We analyzed the SAXS data of this sample with the Unified function [28] (as shown in Fig. 5a), which is suitable for polymeric mass fractals. We note that particle form factor analysis at the highest q is not performed here since the same particles used with that in 43-0.096 sample and their primary particle size and dispersity are discussed in the previous section. Here, we discuss the low and intermediate q-regions in SAXS and SANS data of an aggregated system. With the power law fit at the lowest q region (Fig. 5a), the fractal dimensionality of 2 is deduced, suggesting that particles are connected as Gaussian chains in 84 kg/mol matrix. Correlation length, which is a subunit of cluster, of 8.7 nm is obtained from the intermediate-q region. In 32 kg/mol matrix, the fractal dimension is found as ~ 2.4, indicating a highly branched network of particles. There is also no clear Guinier region in the intermediate-q, so the correlation length for such particle network cannot be obtained.

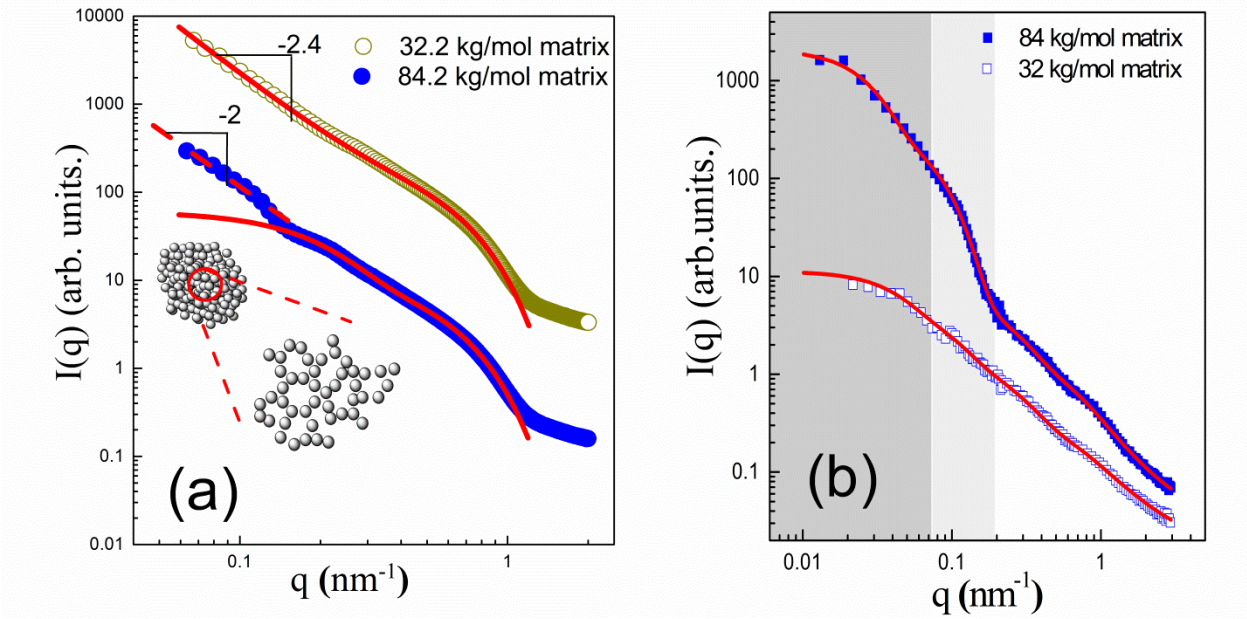

FIG. 5. (Color online) (a) SAXS and (b) SANS profiles of 43 kg/mol PS-grafted nanoparticles with 0.057 chains/nm^2 in 84 (closed symbols) and 32 kg/mol (open symbols) d-PS matrices. Red solid lines are the Beaucage fits. Three-level fitting is applied within shaded q-regions for the sample in 84 kg/mol matrix. Curves are shifted vertically for clarity.

The high-q fitting in SANS data implies the Gaussian conformation of a grafted chain with R_g of 5.6 nm in both matrices (Fig. 5b). This result verifies that chain conformation on low grafted density particles remains unchanged. Robbes et al. [12] reported the collapse of brushes in the linear aggregates of polymer-grafted magnetic nanoparticles. The difference in the shape of their aggregates, -as opposed to spherical aggregates of our system-, lead us to the conclusion that the effect of graft density and also the surface chemistry of individual nanoparticles critically control the physical nature of aggregation and chain conformation within. We compare our SANS data of samples in two different matrices which show significant differences particularly at the low and intermediate-q levels in Fig. 5(b). In 84 kg/mol matrix, the intermediate and low-q regions give a correlation length of 21 nm and cluster size of 63 nm, respectively. This cluster structure

is similar to a network of grafted chains. The power exponent of 2 obtained from the low-q region is also consistent with the fractals of particles that are confirmed in X-ray data. Two-level Beaucage fits for the 32 kg/mol matrix data result in a cluster size of 42 nm and a fractal dimension exponent of 2.4 which is again in-line with the X-ray scattering fit in the low-q region. These results indicate that cluster size is controlled with the penetration of free chains into grafts. The miscibility of free chains into grafted particle networks impedes the collapse of grafted layer even in the aggregated state. We, thus, conjecture that particles can form more compact aggregates in short matrix and more open structures in the longer matrix. The loosely packed aggregates of particles with low graft density (0.057 chains/nm^2) substantiate our recent mechanical results which showed that the composite with spherical aggregated clusters behaved more elastic in the long matrix chains when large oscillatory shear flows were applied [18]. The increase in elastic modulus was attributed to the shear-induced entanglements of the long matrix with 43 kg/mol grafted chains [18]. The scattering results for the same aggregated system suggest that the extent of entanglements determine internal packing characteristics of particles within a cluster, hence shear-induced interfacial stiffening between grafted chains and matrix.

IV. CONCLUSIONS

Nanocomposites of polystyrene-grafted iron oxide nanoparticles at low and intermediate graft densities are studied in SANS, SAXS and TEM techniques. We demonstrate for the first time that at low graft densities, conformations of grafted chains obey Gaussian statistics at different dispersion states. This result reveals grafted chains are not distorted when particles are aggregated into strings, and supports our previous results on the string formation that is controlled with entanglements and attractive interactions between magnetic particles. In the well-dispersed composite, SAXS results indicated good miscibility of particles with matrix chains

where the chain conformations remain Gaussian. Small-angle X-ray scattering and neutron scattering results imply that matrix chains do not influence the strings, but have a significant impact on the size and structure of aggregated particles. For the aggregated system, SAXS and SANS results were in qualitative agreement on the cluster size which suggests that polymer-grafted particles form interpenetrating network-like structures where grafted chains behave Gaussian. The low graft density also allows miscibility of free chains with the particle networks. Varying the molecular mass of matrix polymer influences the structure and size of aggregated particles grafted with short chains. These results present that scattering measurements on particle and polymer parts provide new insight into the internal structures of aggregated polymer-grafted nanoparticles.

ACKNOWLEDGMENTS

We acknowledge financial support from NSF-DMR CAREER grant (#1048865). We thank Dr. Jacques Jestin for discussing the data. We also thank Dr. Paul Butler for his help in SANS experiments. This work utilized facilities supported in part by the National Science Foundation under Agreement No. DMR-0944772. We acknowledge the support of the National Institute of Standards and Technology, U.S. Department of Commerce, in providing the neutron research facilities used in this work. Portions of this work were performed at Beamline X27C at the National Synchrotron Light Source (NSLS), Brookhaven National Laboratory. NSLS is supported by the U.S. Department of Energy, Office of Science, Office of Basic Energy Sciences, under Contract No. DE-AC02-98CH10886.

APPENDIX A: CORRECTION FOR VOID SCATTERING

Figure S1a shows the SANS curve of iron oxide nanoparticles coated with surfactants (*i.e.* bare particles) in d-PS matrix. Two distinct features in the low and high-q regions are apparent which are analyzed separately. The intensity upturn below q < 0.1 nm^{-1} is due to scattering from voids in the composite film. The high-q data arises from the surfactant layers on particles. Thus, total intensity is written as: $I(q) = I_{\text{void}}(q) + I_{\text{surfactant}}(q)$.

Scattering from the surfactants is modelled by similar analysis performed in the grafted chains in the main text. Because bare particles aggregate into spherical clusters in PS matrix, we model the total intensity by applying Percus-Yevick potentials on the fractal objects. The polyshell form factor is used for the surfactant layer around particles. $I_{\text{surfactant}}(q) = P_{polyshell}(q)S_{fractal}(q)S_{P\text{-}Y}(q)$, where $P_{polyshell}(q)$ is the form factor for polydispersed spherical particles with a core-shell structure. $S_{fractal}(q)$ is the intra-cluster structure factor (equation is given on page 13 of the main text). $S_{P\text{-}Y}(q)$ is the Percus-Yevick structure factor and is applied with the Igor software using the definition of $S(q) = 1/1 - C(q)$, where $C(q)$ is the direct correlation function and its approximated expression and exact solution is given in Reference [32]. The black dot line shows the model fit to the high-q data. Surfactant thickness of 0.5 nm and fractal dimension of ~ 3 and the average domain spacing between clusters ~12 nm are obtained from the model analysis.

$I_{surfactant}(q)$ is subtracted from the total intensity to obtain $I_{void}(q)$. Scattering contributions from the voids and grafted chains are represented similarly as the sum of intensities: $I(q) = I_{\text{void}}(q) + I_{\text{grafts}}(q)$. The void scattering is corrected by subtracting $I_{void}(q)$ from the total intensity to get I_{grafts}. SANS profiles before and after void subtraction are shown in Figures S1(b-e).

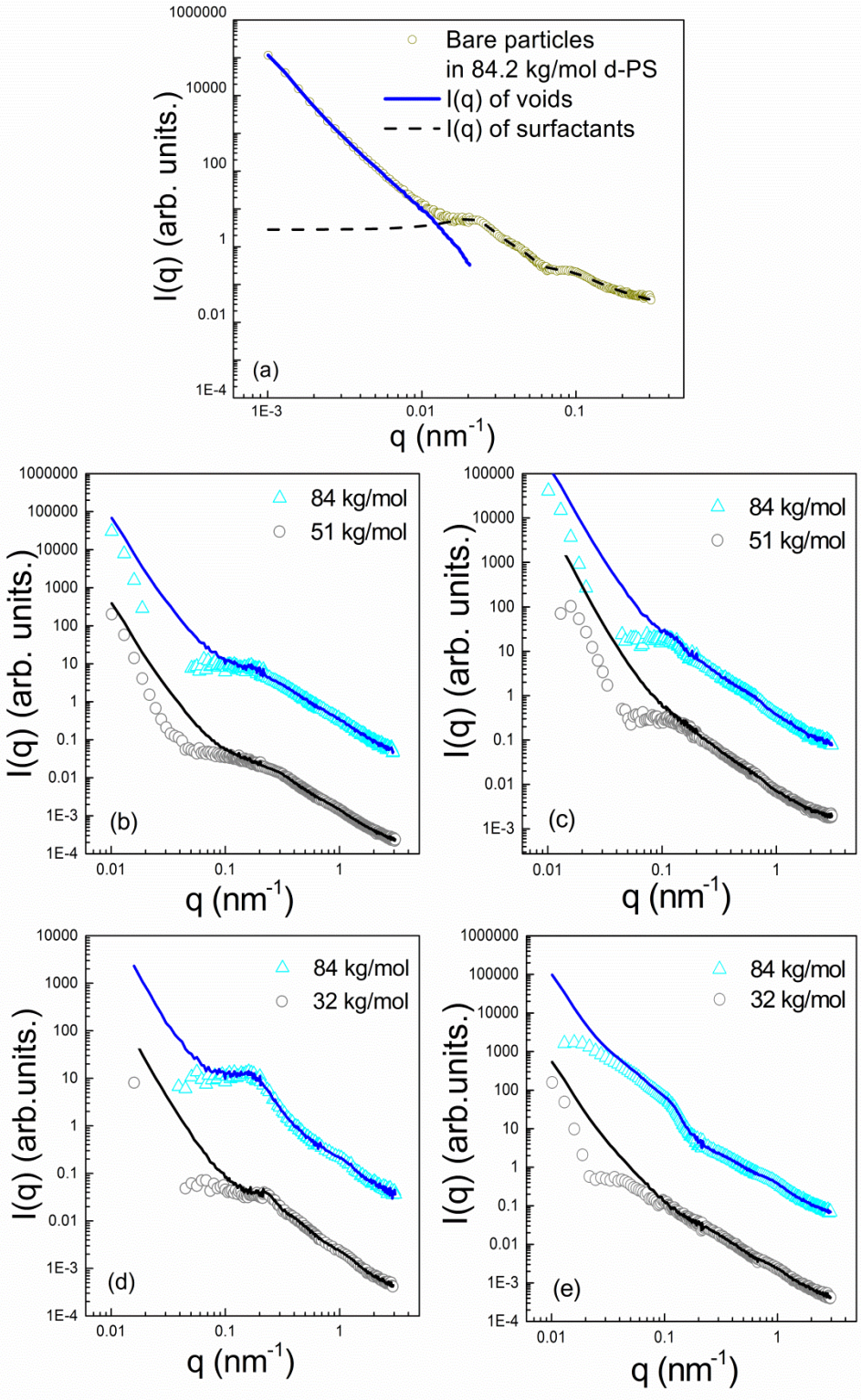
Bare particles
in 84.2 kg/mol d-PS
I(q) of voids
I(q) of surfactants
(a)
I(q) (arb. units.)
q (nm-1)
84 kg/mol
51 kg/mol
(b)
(c)
32 kg/mol
(d)
(e)

FIG. 6. (Color online) (a) SANS of d-PS (84kg/mol) filled with bare particles (green symbols) and the fits for the surfactant layer (dotted black line) and void scattering (blue solid line). (b-e) SANS profiles before (solid lines) and after (open symbols) void subtraction in (b) 100-0.071, (c) 100-0.016, (d) 43-0.096, (e) 43-0.057 samples.

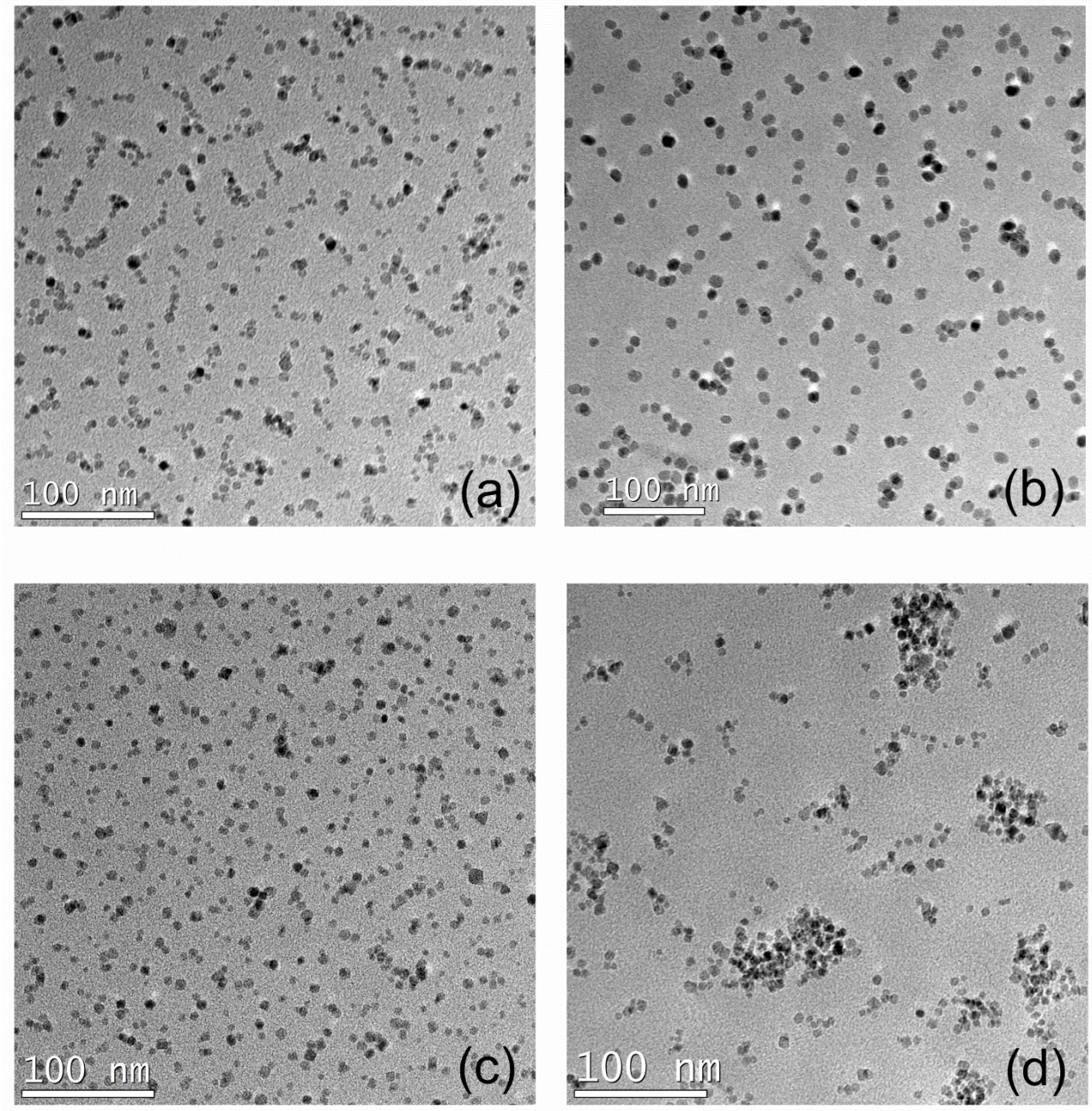

FIG. 7. (Color online) Dispersion of PS-grafted Fe_3O_4 nanoparticles dispersed in short matrix. Matrix molecular weight is 51.6 for (a) 100-0.071 and (b) 100-0.016; and 32.2 kg/mol for (c) 43-0.096 and (d) 43-0.057.

APPENDIX B: MODEL EQUATIONS

Beaucage unified equation [28,33]

$$I(q) = \sum_{i=1}^{N} (G_i e^{\frac{-q^2 R_{g,i}{}^2}{3}} + e^{\frac{-q^2 R_g{}^2}{3}} B_i [(\mathrm{erf}(\frac{qR_{g,i}}{\sqrt{6}})^3 / q)]^{P_i}) + background$$

For each level i, p_i is the power-law exponent that determines the shape of fractals, $R_{g,i}$ is the radius of gyration of structures, q is the scattering vector, A_i and G_i are Guinier and Porod scaling factors, respectively.

Monodispersed sphere form factor [26]

$$P_{sphere}(q,R) = [F_{sphere}]^2$$

$$F_{sphere} = \frac{3[\sin(qR) - qR\cos(qR)]}{(qR)^3}$$ where R is the radius of the sphere.

Cylinder form factor [26]

$$P_{cylinder}(q) = \int_0^{\pi/2} F^2{}_{cylinder}(q,\alpha)\, d\alpha$$

$$F_{cylinder}(q,\alpha) = 2\frac{\sin(qL\cos\alpha/2)}{qL\cos\alpha/2}\frac{J_1(qR\sin\alpha)}{qR\sin\alpha}$$

where R and L are radius and length of a cylinder, respectively.

Polymer excluded volume [24]

The form factor of grafted chain $P_{chain}(q)$ is written as:

$P_{chain}(q) = 2\int_0^1 dx(1-\mathrm{x})\exp[-\frac{q^2a^2}{6}N^{2\nu}\mathrm{x}^{2\nu}]$, where v is the excluded volume parameter, a is the polymer chain statistical segment length and N is the degree of polymerization. Hammouda [24] performed the integration to obtain:

$$P_{chain}(q) = \frac{1}{\nu U^{1/2\nu}}\gamma(\frac{1}{2\nu}, \mathrm{U}) - \frac{1}{\nu U^{1/\nu}}\gamma(\frac{1}{\nu}, \mathrm{U}) .$$

γ(x,U) is the incomplete gamma function: $\gamma(x, \mathrm{U}) = \int_0^U dt \exp(-\mathrm{t})\mathrm{t}^{\mathrm{x}-1}$.

The variable U is given in terms of the scattering variable q as:

$$U = \frac{q^2 a^2 n^{2\upsilon}}{6} = \frac{q^2 R_g{}^2 (2\nu+1)(2\nu+2)}{6}$$

The radius of gyration squared has been defined as:

$$R_g{}^2 = \frac{a^2 n^{2\nu}}{(2\nu+1)(2\nu+2)}$$

Core-chain and Chain-Chain Structure Factors in the Pedersen Model [34]

The correlation between the particle core and a grafted chain is given by:

$$S_{core-chain}(q) = f_{sphere}(q,R) f_{chain} \frac{\sin[q(R_g + R)]}{q(R_g + R)}, \text{ where } f_{chain} = \frac{1 - \exp(-q^2 R_g{}^2)}{q^2 R_g{}^2}.$$

The correlation between grafted chains is given by:

$$S_{chain-chain}(q) = f_{chain}{}^2 [\frac{\sin(q(R + R_g))}{q(R + R_g)}]^2$$

[1] N. Jouault, D. Lee, D. Zhao and S. K. Kumar, Advanced Materials **26**, 4031 (2014).
[2] N. Jouault, J. F. Moll, D. Meng, K. Windsor, S. Ramcharan, C. Kearney and S. K. Kumar, ACS Macro Lett. **2**, 371 (2013).
[3] E. Senses and P. Akcora, Macromolecules **46**, 1868 (2013).
[4] S. K. Kumar, N. Jouault, B. Benicewicz and T. Neely, Macromolecules **46**, 3199 (2013).
[5] P. Akcora, H. Liu, S. K. Kumar, J. Moll, Y. Li, B. C. Benicewicz, L. S. Schadler, D. Acehan, A. Z. Panagiotopoulos, V. Pryamitsyn*, et al.*, Nature Materials **8**, 354 (2009).
[6] Y. Jiao and P. Akcora, Macromolecules **45**, 3463 (2012).
[7] M. K. Crawford, R. J. Smalley, G. Cohen, B. Hogan, B. Wood, S. K. Kumar, Y. B. Melnichenko, L. He, W. Guise and B. Hammouda, Phys. Rev. Lett. **110**, 196001 (2013).
[8] D. Bedrov, G. D. Smith and L. Li, Langmuir **21**, 5251 (2005).
[9] T. Lafitte, S. K. Kumar and A. Z. Panagiotopoulos, Soft Matter **10**, 786 (2014).
[10] D. Meng, S. K. Kumar, J. M. D. Lane and G. S. Grest, Soft Matter **8**, 5002 (2012).
[11] C. Chevigny, F. Dalmas, E. Di Cola, D. Gigmes, D. Bertin, F. Boué and J. Jestin, Macromolecules **44**, 122 (2011).
[12] A. S. Robbes, F. Cousin, F. Meneau, F. Dalmas, R. Schweins, D. Gigmes and J. Jestina, Macromolecules **45**, 9220 (2012).
[13] C. Chevigny, J. Jestin, D. Gigmes, R. Schweins, E. Di-Cola, F. Dalmas, D. Bertin and F. Boué, Macromolecules **43**, 4833 (2010).
[14] G. G. Vogiatzis and D. N. Theodorou, Macromolecules **46**, 4670 (2013).
[15] J. Choi, H. Dong, K. Matyjaszewski and M. R. Bockstaller, J. Am. Chem. Soc. **132**, 12537 (2010).
[16] M. J. A. Hore, J. Ford, K. Ohno, R. J. Composto and B. Hammouda, Macromolecules **46**, 9341 (2013).
[17] J. S. Pedersen and M. C. Gerstenberg, Macromolecules **29**, 1363 (1996).
[18] E. Senses, Y. Jiao and P. Akcora, Soft Matter **10**, 4464 (2014).
[19] L. Noirez, H. Mendil-Jakani and P. Baroni, Macromolecular Rapid Communications **30**, 1709 (2009).
[20] S. Sun, H. Zeng, D. B. Robinson, S. Raoux, P. M. Rice, S. X. Wang and G. Li, Journal of the American Chemical Society **126**, 273 (2004).
[21] M. L. Jung, H. K. Ok, E. S. Sang, B. H. Lee and S. Choe, Macromolecular Research **13**, 236 (2005).
[22] Y. Yang, Z. Yang, Q. Zhao, X. Cheng, S. C. Tjong, R. K. Y. Li, X. Wang and X. Xie, J. Polym. Sci. A Polym. Chem. Ed. **47**, 467 (2009).
[23] S. R. Kline, J. Appl. Cryst. **39**, 895 (2006).
[24] B. Hammouda, *Polymer Characteristics* (Springer Berlin Heidelberg, Berlin Heidelberg, 1993), pp. 87.
[25] J. S. Pedersen, J. Chem. Phys. **114**, 2839 (2001).
[26] A. Guinier, G. Fournet, C. B. Walker and K. L. Yudowitch, *Small-angle scattering of X-rays*. (Wiley, New York, 1955).
[27] J. Ilavsky and P. R. Jemian, J. Appl. Cryst. **42**, 347 (2009).
[28] G. Beaucage, J. Appl. Cryst. **29**, 134 (1996).
[29] M. Wertheim, Phys. Rev. Lett. **10**, 321 (1963).
[30] J. K. Percus and G. J. Yevick, Physical Review **110**, 1 (1958).
[31] J. Teixeira, J. Appl. Cryst. **21**, 781 (1988).
[32] M. S. Wertheim, Physical Review Letters **10**, 321 (1963).

[33] B. Hammouda, Journal of Applied Crystallography **43**, 1474 (2010).
[34] J. S. Pedersen and M. C. Gerstenberg, Macromolecules **29**, 1363 (1996).